



Cite this: *Org. Biomol. Chem.*, 2020, **18**, 6519

## *N*-Methyl- $\beta$ -carboline alkaloids: structure-dependent photosensitizing properties and localization in subcellular domains<sup>†</sup>

M. Paula Denofrio,<sup>‡a</sup> Federico A. O. Rasse-Suriani,<sup>‡a,b</sup> Jose M. Paredes,<sup>c</sup> Federico Fassetta,<sup>a</sup> Luis Croveto,<sup>†d</sup> \*<sup>c</sup> Maria D. Giron,<sup>d</sup> Rafael Salto,<sup>d</sup> Bernd Epe<sup>e</sup> and Franco M. Cabrerizo<sup>†d</sup> \*<sup>a</sup>

*N*-Methyl- $\beta$ -carboline ( $\beta$ C) alkaloids, including normelinonine F (**1b**) and melinonine F (**2b**), have been found in a vast range of living species playing different biological, biomedical and/or pharmacological roles. Despite this, molecular bases of the mechanisms through which these alkaloids would exert their effect still remain unknown. Fundamental aspects including the photosensitizing properties and intracellular internalization of a selected group of *N*-methyl- $\beta$ C alkaloids were investigated herein. Data reveal that methylation of the  $\beta$ C main ring enhances its photosensitizing properties either by increasing its binding affinity with DNA as a biomolecular target and/or by increasing its oxidation potential, in a structure-dependent manner. As a general rule, *N*(9)-substituted  $\beta$ Cs showed the highest photosensitizing efficiency. With the exception of 2-methyl-harminium, all the *N*-methyl- $\beta$ Cs investigated herein induce a similar DNA photodamage profile, dominated largely by oxidized purines. This fact represents a distinctive behavior when comparing with *N*-unsubstituted- $\beta$ Cs. On the other hand, although all the investigated compounds might accumulate mainly into the mitochondria of HeLa cells, methylation provides a distinctive dynamic pattern for mitochondrial uptake. While rapid (passive) diffusion is most probably responsible for the prompt uptake/release of neutral  $\beta$ Cs, an active transport appears to mediate the (relatively slow) uptake of the quaternary cationic  $\beta$ Cs. This might be a consequence of a distinctive subcellular localization (mitochondrial membrane and/or matrix) or interaction with intracellular components. Biomedical and biotechnological implications are also discussed herein.

Received 31st May 2020,

Accepted 1st July 2020

DOI: 10.1039/d0ob01122c

rsc.li/obc

## Introduction

$\beta$ -Carbolines ( $\beta$ Cs) are a set of endogenous alkaloids present in a vast range of living species.<sup>1–8</sup> The  $\beta$ C skeleton construction

occurs through the catalysed Pictet–Spengler reaction.<sup>9–11</sup> In particular, *N*-methyl- $\beta$ -carboline alkaloids, including normelinonine F (**1b**) and melinonine F (**2b**), were isolated from different mammals' body tissues and fluids such as brain, cerebrospinal and plasma.<sup>1–7</sup> A broad spectrum of biological, biomedical and pharmacological activities has been reported for these alkaloids:

(i) unsubstituted full aromatic norharmane (**1a**) crosses the blood–brain barrier penetrating into the brain,<sup>12,13</sup> where it is enzymatically converted into the quaternary  $\beta$ Cs **1b** and 2,9-dimethyl-norharmanium (**1d**).<sup>14</sup>

(ii) **1b**, **1d** and other related quaternary  $\beta$ Cs were described as potential pathogenic agents in several neurological disorders, including Parkinson's disease.<sup>15–17</sup> The main mechanism through which these alkaloids would exert their effect seems to be the mitochondrial respiratory inhibition.<sup>18</sup>

(iii) **1b** was also found to be a potent inhibitor of acetylcholinesterase (AChE), a target for the clinical treatment of Alzheimer and other memory impairments of vascular origin.<sup>19</sup>

<sup>a</sup>Instituto Tecnológico de Chascomús (INTECH), Universidad Nacional de San Martín (UNSAM) - Consejo Nacional de Investigaciones Científicas y Técnicas (CONICET), Av. Intendente Marino Km 8.2, CC 164 (B7130IWA) Chascomús, Argentina. E-mail: fcabrerizo@intech.gov.ar

<sup>b</sup>Instituto de Investigaciones Físicoquímicas Teóricas y Aplicadas (INIFTA), CCT-La Plata, Universidad Nacional de La Plata, Diag. 113 y 64 (1900), La Plata, Argentina

<sup>c</sup>Department of Physical Chemistry, Faculty of Pharmacy, Unidad de Excelencia en Química Aplicada a Biomedicina y Medioambiente (UEQ), University of Granada, Cartuja Campus, 18071 Granada, Spain. E-mail: luiscroveto@ugr.es

<sup>d</sup>Department of Biochemistry and Molecular Biology II, Faculty of Pharmacy, Unidad de Excelencia en Química Aplicada a Biomedicina y Medioambiente (UEQ), University of Granada, Cartuja Campus, 18071 Granada, Spain

<sup>e</sup>Institute of Pharmacy and Biochemistry, University of Mainz, Staudingerweg 5, Mainz, Germany

<sup>†</sup>Electronic supplementary information (ESI) available. See DOI: 10.1039/d0ob01122c

<sup>‡</sup>Equal contribution of both authors



(iv) on the contrary, 9-methyl-norharmane (**1c**) would exert neuroprotective and neuron-differentiating effects.<sup>20</sup>

(v)  $\beta$ C derivatives having a short alkyl or benzyl substituent at position N(9) were found to be promising antitumor and antiproliferative agents. Compounds substituted at both N(9) and C(3) positions showed a remarkable enhancement of the antitumor activity with a concomitant decrease in the acute toxicity and neurotoxicity. The magnitude and extent of the latter effects strongly depend on the chemical nature of substituents.<sup>21</sup>

(vi) *N*-Methyl- $\beta$ Cs are also quite promising antimicrobial agents with remarkable activity against a great variety of microorganisms.<sup>22–36</sup> For example, **1b** and **2b** showed anti-*Plasmodium* activity, even against the chloroquine- and pyrimethamine-resistant *Plasmodium falciparum* K1 type.<sup>32,33</sup> In addition, **1b** and its chloro-derivatives displayed potent cyanobactericidal and algicidal activity against a group of photosynthetic aquatic organisms including *Microcystis aeruginosa*, *Synechococcus* sp. and *Kirchneriella contorta*.<sup>34</sup> In a very recent study, several  $\beta$ C derivatives were identified as novel and potent antiviral agents against *Herpes simplex*-1 and -2 virus. In particular, 9-methyl-derivatives **1c** and **2c** showed the highest inhibitory effect on virus replication.<sup>35</sup> The mechanism of action appears to be at the transcriptional level where these alkaloids could bind to the viral genome and block transcription, giving rise to a delay (or even suppression) in the early and late protein expression.<sup>35,36</sup> Interestingly, **1c** and **2c** could also play a role at the post-translational level, interfering with the late location of HHV infected cell polypeptide 0 (ICP0) at the cytoplasm where this protein normally inhibits antiviral signalling and promotes viral replication.

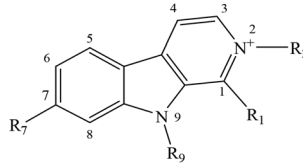
(vii) Due to their planar chemical structure, most of the  $\beta$ Cs<sup>37–40</sup> including **1b** and **2b** interact with DNA.<sup>41</sup> Partial intercalation of the indolic ring into the stacked base-pairs is the dominant mode of interaction, placing the  $\beta$ C-pyridine ring in a polar-protic environment.<sup>37–40</sup>

(viii) The photosensitizing properties of a selected group of  $\beta$ C alkaloids have been demonstrated on both cell-free and intracellular DNA and its components.<sup>37–40,42–46</sup> Interestingly, harmine (**3a**)<sup>38</sup> as well as **3c**<sup>40</sup> and chloro-harmine derivatives<sup>39</sup> were shown to be the most efficient photosensitizers among all the  $\beta$ Cs investigated to date. Thus, the methoxy group placed at position C(7) would play a key role enhancing the photosensitizing properties of the  $\beta$ C ring.

On the other hand, the broad variety of tuneable physico-chemical and photochemical properties of  $\beta$ Cs make these alkaloids quite a promising set of molecules for a great variety of biotechnological applications. Recently,  $\beta$ Cs were used as photosensitizer agents and fluorescence markers carried by selective vehicles, based on albumin-folate conjugates, for tumour cell targeted PDT.<sup>45</sup> Although encouraging results were obtained, the overall photodynamic efficiency depicted was relatively low. Thus, the search for novel and more efficient photosensitizers based on small and biocompatible molecules is still a challenge.

Despite the well-established biological and biomedical relevance of *N*-methyl- $\beta$ Cs, the molecular bases of the mecha-

**Table 1** Chemical structures of  $\beta$ -carbolines studied in the present work



Short name (abbreviation)	R <sub>1</sub>	R <sub>2</sub>	R <sub>7</sub>	R <sub>9</sub>
Norharmane ( <b>1a</b> )	-H	-H	-H	-H
2-Methyl-norharmanium or normelinone F ( <b>1b</b> )	-H	-CH <sub>3</sub>	-H	-H
9-Methyl-norharmane ( <b>1c</b> )	-H	-H	-H	-CH <sub>3</sub>
2,9-diMethyl-norharmanium ( <b>1d</b> )	-H	-CH <sub>3</sub>	-H	-CH <sub>3</sub>
Harmane ( <b>2a</b> )	-CH <sub>3</sub>	-H	-H	-H
2-Methyl-harmanium or melinone F ( <b>2b</b> )	-CH <sub>3</sub>	-CH <sub>3</sub>	-H	-H
9-Methyl-harmane ( <b>2c</b> )	-CH <sub>3</sub>	-H	-H	-CH <sub>3</sub>
2,9-diMethyl-harmanium ( <b>2d</b> )	-CH <sub>3</sub>	-CH <sub>3</sub>	-H	-CH <sub>3</sub>
Harmine ( <b>3a</b> )	-CH <sub>3</sub>	-H	-OCH <sub>3</sub>	-H
2-Methyl-harminium ( <b>3b</b> )	-CH <sub>3</sub>	-CH <sub>3</sub>	-OCH <sub>3</sub>	-H
9-Methyl-harmine ( <b>3c</b> )	-CH <sub>3</sub>	-H	-OCH <sub>3</sub>	-CH <sub>3</sub>
2,9-diMethyl-harminium ( <b>3d</b> )	-CH <sub>3</sub>	-CH <sub>3</sub>	-OCH <sub>3</sub>	-CH <sub>3</sub>

nisms through which these alkaloids would exert their effect still remain unclear. To gain further insight with these regards, fundamental aspects including the photosensitizing properties as well as the intracellular internalization of a selected group of *N*-methyl- $\beta$ C alkaloids (Table 1) were investigated herein.

## Experimental

### General

**Reactants.** Norharmane (>98%), harmane (>98%) and harmine (>98%) from Sigma-Aldrich were used without further purification. *N*-Methyl- $\beta$ -carboline derivatives were synthesized, purified and characterized according to the procedure described elsewhere.<sup>7</sup> DNA from bacteriophage PM2 (PM2 DNA, 10<sup>4</sup> bp) was prepared according to the method of Salditt *et al.*<sup>47</sup> Calf thymus DNA (ctDNA, sodium salt type I, highly polymerized, Lot no. 105K7025) and 2'-deoxyadenosine 5'-monophosphate (dAMP) were provided by Sigma-Aldrich. PlasmaCAL Phosphorus (SPC Science, Standard for ICP-EAS and -MS, 995 ( $\pm$ 4)  $\mu$ g ml<sup>-1</sup> H<sub>2</sub>O,  $\delta$  = 1.000 g ml<sup>-1</sup> @ 23.4 °C).

**Enzymes.** Formamidopyrimidine-DNA glycosylase (Fpg) was obtained from *E. coli* strain JM105 harbouring plasmid pFPG230.<sup>48</sup> Endonuclease IV (Endo IV) and T4 endonuclease V (T4 endo V) were partially purified from an inducible overproducer (*E. coli* strain A 32 480 carrying the plasmid ptac-denV) provided by L. Mullenders, Leiden. Endonuclease III (Endo III) from *E. coli* was kindly provided by S. Boiteux, Fontenay aux Roses, France. All repair endonucleases were tested for their incision at reference modifications according to the procedure described elsewhere.<sup>49</sup>

**Cell cultures and preparations.** Human epithelioid cervix carcinoma (HeLa, ATCC: CCL-2) and HEK293 cells (ATCC:



CRL-1573) were provided by the Cell Culture Facility of the University of Granada. Cell cultures were grown at 37 °C in a humidified 5% CO<sub>2</sub> incubator in Dulbecco's Modified Eagle's Medium (DMEM) supplemented with 10% (v/v) fetal bovine serum (FBS), 2 mM glutamine, 100 U mL<sup>-1</sup> penicillin, and 0.1 mg mL<sup>-1</sup> streptomycin. Cells were seeded in 6-well plates with a density of 225 000 cells per cm<sup>2</sup> on 25 mm coverslips to reach a 70–80% confluence. (i) *Cells preparation for FLIM microscopy experiments*: HeLa and HEK239 cells were washed (2 times) with phosphate buffered saline medium (PBS) and incubated during 5, 10, 15, 20 or 35 min with PBS and the corresponding βC (10 μM) at 37 °C. (ii) *Cells preparation for colocalization studies*: HeLa cells in DMEM free of FBS were first incubated with 16 nM of Mitotracker® and LysoTracker® in two different sets of experiments. After 20 min of incubation, **1d** (10 μM) was added and co-incubated during 2 h. Cells were then washed (3 times) with PBS and fixed using filtered paraformaldehyde (2%). Fixed samples were again washed (3 times) with PBS and prepared for confocal microscope analysis.

### Calf thymus DNA (ctDNA) absorption coefficient determination

**Stock solutions preparation.** dAMP was dissolved in freshly degassed Milli-Q (Millipore) water, whereas up to 2 mg mL<sup>-1</sup> ctDNA was reconstituted in Tris (10 mM) with EDTA (1 mM) at pH 7.5–8.0, following the standard procedure recommended by the supplier. Stock solutions were prepared and stored, at 4 °C, in sealed glass tubes in order to avoid the adsorption of the genetic material on plastic surfaces. To reduce further shearing of the ctDNA, gentle inversion overnight at 0 °C–4 °C was used to completely solubilize the ctDNA. ctDNA stock solution was divided in three fractions and sealed. The first fraction was used without further purification and the last two fractions were dialyzed against Milli-Q (Millipore) water<sup>50</sup> and ammonium chloride (10 mM NH<sub>4</sub>Cl, pH 7.4)<sup>51</sup> aqueous solution, respectively, prior to phosphorus analysis. Note that although the starting ctDNA material used was of the highest available purity (>98%), dialysis was performed to further remove any potential additional phosphate source. Dialysate solvent was replaced up to seven times and a dialysis tubing cellulose membrane (Sigma-Aldrich, with average flat width of 25 mm, M. W. 11 241) was used as dialysis membrane.

**Samples preparation for molar absorption coefficients (ε) determination.** Serial dilutions of ctDNA and dAMP stock solutions were made in different solvents according to each experiment (see below) and sealed, leading to dilution factors (*D*) ranging 2–8. Final pH values were verified to lie between 6.9 and 7.2. From each sample solution UV-visible spectra and phosphorus content ([P]) were determined following the procedure described below. The molar absorption coefficient was calculated from the slope of the linear plot between corrected absorbance  $A_{\text{cor}}^{260\text{nm}}$  (defined as the absorbance normalized at 1 cm optical pathlength) and [P].

**UV-visible absorption spectroscopy.** UV absorbance was measured on a PerkinElmer L25 spectrophotometer blanked against water or 10 mM ammonium chloride aqueous solu-

tion. Measurements were carried out in quartz cuvettes with 1 mm, 4 mm or 10 mm pathlengths, in order to keep the absorbance readings within the linear region of the Lambert–Beer law ( $A^{260\text{ nm}}$  range 0.10–1.20). UV-visible absorption measurements were made on the same day as phosphate quantification in order to minimize potential sources of error such as changes in the relative concentration due to evaporation and/or sample degradation or microbial contamination.

**Microwave plasma – emission atomic spectroscopy (MP-EAS).** Total phosphorus analyses of ctDNA samples were performed with an Agilent 4200 MP-AES equipment, consisting of a microwave induced plasma interfaced to an atomic emission spectrophotometer, using nitrogen extracted from ambient air. ctDNA and dAMP aqueous samples were nebulized prior to interaction with the plasma. The viewing position and nebulizer pressures were optimized automatically using the Agilent MP Expert software. Instrumental parameters used for sample analysis were wavelengths 213.618 nm, 214.915 nm, 253.560 nm and 255.326 nm (four different wavelengths were selected in order to provide wide dynamic range and to avoid spectral interferences); read time = 3 s, replicates = 3; nebulizer flow = 0.35 L min<sup>-1</sup>, background correction = automatically; pump speed 15 rpm, sample introduction = manual; uptake time = 15 s (fast pump); stabilization time = 15 s; number of pixels = 3. Samples were prepared according to the above description.

**Analytical calibration.** Rational calibration fit was a non-linear curve fit,  $y = (ax - b)/(1 + cx)$ , in order to work in an extended dynamic range. Samples with analyte concentrations that exceed the maximum concentration used in the calibration curve were diluted accordingly and analysed again. The acceptance criterion for calibration curve correlation coefficient is 0.99995. At least four calibration standards, excluding the calibration blank, were used for calibration. A typical calibration curve is depicted in ESI Fig. 2.†

The method was validated by determining the molar absorption coefficient at 260 nm ( $\epsilon^{260\text{ nm}}$ ) of 2'-deoxyadenosine 5'-monophosphate (dAMP) in aqueous solution (ESI Fig. 2c and d†). When comparing data obtained herein ( $15.824 \pm 30\text{ M}^{-1}\text{ cm}^{-1}$ ) with the gravimetrically obtained value ( $15.060\text{ M}^{-1}\text{ cm}^{-1}$ )<sup>52</sup> a relative error of ~4% was observed.

### Binding studies

The interaction of βC derivatives with ctDNA, in KH<sub>2</sub>PO<sub>4</sub>–NaOH (pH 7.4, 10 mM) buffer solutions, was studied by both steady-state and time-resolved fluorescence spectroscopy. Equipment and data analysis used were described elsewhere.<sup>40</sup> The use of ctDNA as a model of genetic material allows a direct comparison with the information reported in the literature for related βCs.<sup>38–40,44</sup>

### DNA photoproduct measurements

**Irradiation set-up.** A mixture of βC buffered aqueous solutions (10 mM KH<sub>2</sub>PO<sub>4</sub>, 50 mM NaCl, pH 7.4) and PM2 DNA (at 10 μg mL<sup>-1</sup>) were irradiated for 20 min on ice in a 96 well-plate with a UVA Philips HPW 125 W lamp emitting at 365 (±20) nm,



placed at a distance of 10 cm. Note that at these excitation wavelengths all the investigated  $\beta$ Cs show quite high absorption coefficients,  $\epsilon$ ,<sup>7,53</sup> whereas DNA absorption is negligible. Treated DNA was precipitated by ethanol/sodium acetate and subsequently dissolved in BE1 buffer (20 mM Tris-HCl, pH 7.5; 0.1 M NaCl and 1 mM EDTA) for damage analysis.

**Quantitative analysis of endonuclease-sensitive modifications.** The DNA relaxation assay used to quantify the number of photoinduced endonuclease-sensitive sites (ESS) and single-strand breaks (SSB) in PM2 DNA has been described earlier.<sup>54,55</sup> It makes use of the fact that supercoiled PM2 DNA is converted by either a SSB or the incision of a repair endonuclease into a relaxed (nicked) form, which migrates separately from the supercoiled form in agarose gel electrophoresis. Its application to characterize the DNA damage induced by photosensitization as well as the type of repair enzymes and experimental conditions have been previously described in detail.<sup>40</sup>

The number of cyclobutane pyrimidine dimers (CPDs<sup>calc</sup>) were calculated as the difference between the number of sites recognized during incubation with both Endo IV and T4 endo V and the number of AP sites recognized by Endo IV alone. Likewise, the number of oxidatively generated damage on pyrimidine nucleobases (Ox-Py<sup>calc</sup>) were calculated by combining the use of both Endo III and Endo IV enzymes. To further identify the photosensitized DNA damage, two different control experiments were carried out: *light-controls* (PM2 DNA irradiated in the absence of *N*-methyl- $\beta$ Cs) and *dark-controls* (mixtures of PM2 and *N*-methyl- $\beta$ Cs, at the highest concentrations, kept in the dark).

### Fluorescence imaging microscopy

*FLIM experiments* were carried out on a MicroTime 200 instrument (PicoQuant), using a LDH-375 (PicoQuant) pulsed laser as the excitation source with a repetition rate of 20 MHz. The laser was directed into the sample using a dichroic mirror (F33-375RDC, AHF/Chroma) and an oil immersion objective (1.4 NA, 100 $\times$ ) of an inverted microscope (IX-71, Olympus). The emitted fluorescence was filtered by a cutoff filter (F76-405LP, AHF/Chroma) and focused onto a 75  $\mu$ m pinhole. The detection filter was a FB450-40 bandpass filter (Thorlabs), and the fluorescence was detected using a single-photon avalanche diode (SPCM-AQR 14, PerkinElmer). Photon counting, imaging reconstruction and data acquisition were performed with a TimeHarp 200 TCSPC module (PicoQuant). Raster scanned images were recorded with a 512  $\times$  512 pixels resolution. The fluorescence images were analyzed using the image processing package Fiji.<sup>56</sup>

*Colocalization studies* were performed in a Leica SPS II confocal microscope equipped with a 405 nm diode laser and 633 nm HeNe laser. Excitations were sequentially switched between 405 and 633 nm, to pump **1d** and the biomarkers, respectively. Emission signals were recorded in two different emission ranges: 410–490 and 640–750 nm, to collect **1d** (cyan channel) and the red the biomarkers (red channel) fluorescent emission, respectively. The objective used was a PL APO 63x/

1.2 CS water immersion. Fluorescence was acquired using a hybrid detector (HyD, Leica).

## Results and discussion

### DNA damage photoinduced by *N*-methyl- $\beta$ Cs

The photosensitizing properties of a set of *N*-methyl- $\beta$ Cs (Table 1) were explored herein using supercoiled extracellular DNA of bacteriophage PM2. DNA shows several sites of attack leading place to a broad spectrum of chemical reactions. The use of the latter DNA model, in combination with a set of incision repair endonucleases, allows the evaluation of all types of putative photosensitizing mechanisms.<sup>39</sup> PM2 DNA was subject to UVA (365 nm) irradiation, in the presence of different concentrations of *N*-methyl- $\beta$ Cs. The number of single-strand breaks (SSBs) as well as DNA modifications recognized by the DNA repair glycosylase Fpg, which are mainly oxidatively modified purines (8-oxo-7,8-dihydroguanine and formamidopyrimidines) and sites of base loss (AP sites), were subsequently quantified (Fig. 1, left column). Similar dose-dependencies have already been reported for other related  $\beta$ Cs.<sup>37–40,44,45,57</sup> Briefly, the number of DNA modifications increases linearly with the compounds' concentration. For all the investigated alkaloids Fpg-sensitive sites were found to be produced with the highest efficiency, whereas SSBs were produced with a very low or even null efficiency (<0.07 modifications/10<sup>4</sup> bp). Note that all DNA damage is mediated by the photoexcited  $\beta$ Cs, since no damage was observed in both *light-control* (see data points at the y-intercept in Fig. 1a, left column) and *dark-controls* (see the empty stars at the maximum  $\beta$ C concentration depicted in Fig. 1a, left column).

Since  $\beta$ Cs can lead to the formation of a wide range of DNA photoproducts,<sup>38,39</sup> DNA damage profiles (*i.e.*, the number of various other types of repair enzymes-sensitive modifications) photoinduced by *N*-methyl- $\beta$ Cs were also determined (Fig. 1, right column). In particular, four different repair endonucleases were used to selectively quantify different type of DNA modifications: • Fpg to detect oxidatively damaged purines and AP-sites (see above), • Endo III to recognize oxidized pyrimidines as well as AP sites, • T4 endo V to recognize cyclobutane pyrimidine dimers (CPDs) and a number of specific types of AP-sites, and • Endo IV to sense all types of AP-sites.

Data depict qualitative and quantitative structure–activity relationships:

(i) with the exception of **3b**, all the *N*-methyl-derivatives investigated induce specific DNA base damage. *I. e.*, Fpg-sensitive modifications represent the main types of photoproducts, while oxidized pyrimidines (Ox-Py<sup>calc</sup>) as well as CPDs and SSBs are absent or generated in low relative yields. This contrasts with the DNA damage spectra previously determined for unsubstituted  $\beta$ C rings (**1a**, **2a** and **3a**), which induce a broader spectrum of DNA modifications (ESI Fig. 1†).<sup>38</sup> It is generally accepted that Fpg-sensitive sites are produced either by type I or type II photosensitization mechanisms. It was demonstrated that the methylation of  $\beta$ Cs' ring has no signifi-



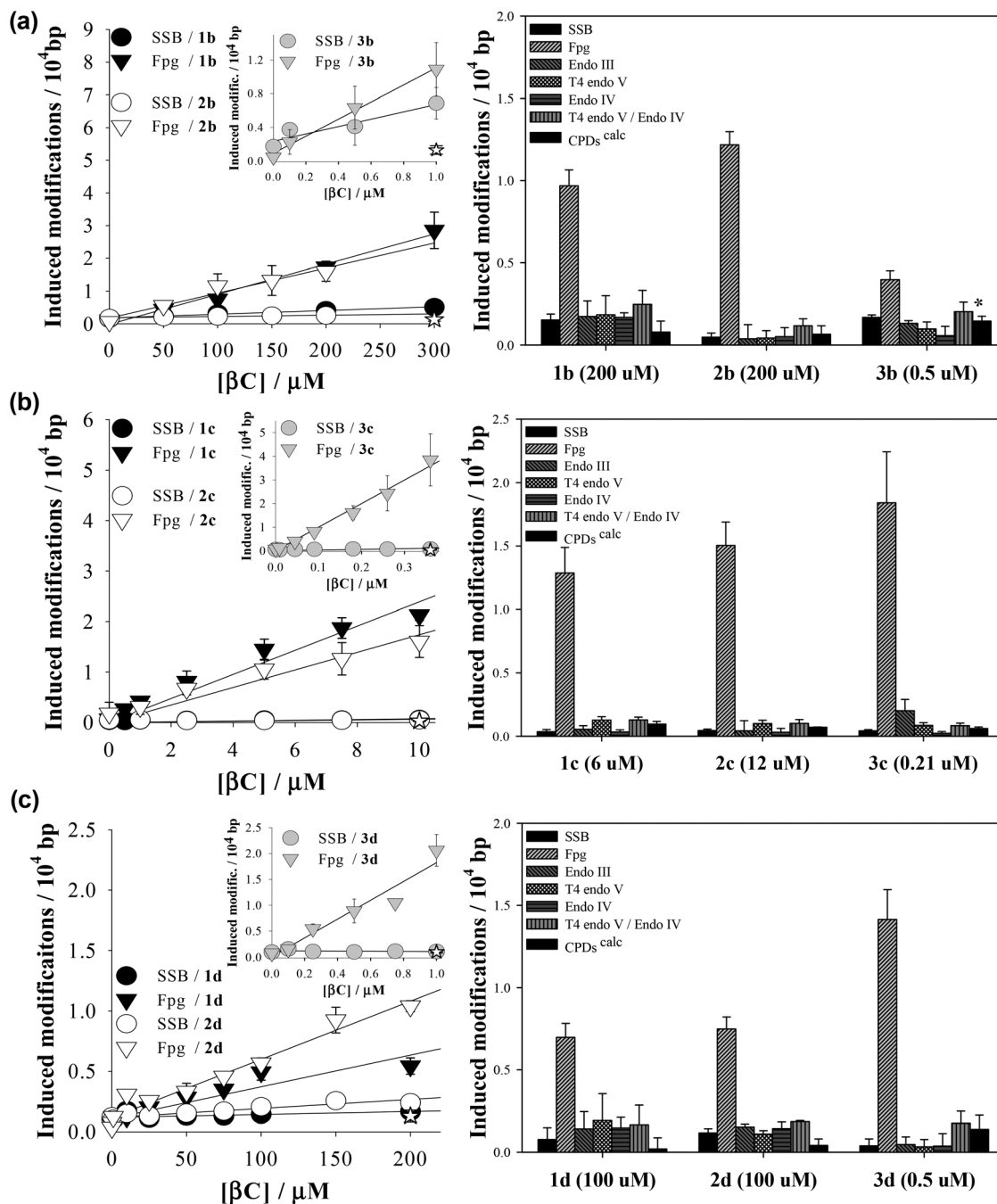


**Fig. 1** Left column: SSBs (circles) and Fpg-sensitive modifications (down triangles) induced in PM2 DNA by exposure to UVA light ( $366 \pm 20$  nm; 20 minutes) in the presence of different concentrations of (a) 2-methyl- $\beta$ Cs, (b) 9-methyl- $\beta$ Cs and (c) 2,9-dimethyl- $\beta$ Cs in phosphate buffer solutions (pH 7.4). Right column: DNA damage profiles showing the numbers of SSBs and several types of endonuclease sensitive modifications induced in PM2 DNA by photoexcited *N*-methyl- $\beta$ Cs. The concentrations are indicated in parenthesis. Data are the means of 5 independent experiments ( $\pm$ S.D.).

cant effect on the intrinsic capability to photosensitize reactive oxygen species (ROS) formation<sup>7</sup> but shifts the oxidation potential of the  $\beta$ C main ring towards more positive values.<sup>58</sup> In addition, electronic excited  $\beta$ Cs show a characteristic separation of charge. Thus, as it was demonstrated for *N*(9)-methyl  $\beta$ Cs (**1c**, **2c** and **3c**),<sup>40</sup> electron/proton exchanges (type I oxidative processes) would be enhanced and, hence, the formation of Fpg-sensitive sites. Among the nucleobases, guanine

is the most susceptible target of an oxidative attack, both by type I and type II mechanism.

(ii) On the contrary, **3b** showed a broader damage profile. A close look at the data reveals that the yield of oxidized purines (8-oxoG) is reduced relative to that of AP-sites, oxidized pyrimidines as well as CPDs. It has been demonstrated that photo-sensitized formation of CPDs mainly occurs through triplet-triplet energy transfer (TTET) from the triplet electronic



excited state of the photosensitizer to the triplet electronic state of the pyrimidine (mostly, thymine). This process is thermodynamically favoured for those photosensitizers having energy triplet values ( $E_T$ ) larger than  $267 \text{ kJ mol}^{-1}$ .<sup>59</sup> Although the  $E_T$  value of **3b** was not determined, it was demonstrated that the unsubstituted derivative **3a** has the required energy ( $274.4 \text{ kJ mol}^{-1}$ ).<sup>60</sup>

Considering that methylation at position N(2) induces an only small change in the relative energy of the electronic states (*i.e.*, bathochromic shift  $\sim 5 \text{ nm}$ ), it is expected that **3b** also has the required energy for triplet-triplet sensitization. This hypothesis should be further investigated.

(iii) The 9-methyl-derivatives (**1c**, **2c**, **3c**) show a higher photosensitizing efficiency than the corresponding cationic species (*i.e.*, ten-times lower concentrations of 9-methyl- $\beta$ Cs give rise to a similar amount of DNA damage as 2-methyl- $\beta$ Cs and 2,9-dimethyl- $\beta$ Cs). This fact can be accounted for by the lower polarity of the 9-methyl- $\beta$ C molecules that can give rise to a higher hydrophobic interaction with the DNA double helix (partial intercalation). On the other hand, the positive net charge placed on the 2-methyl- and 2,9-dimethyl- $\beta$ C cationic species would enhance their electrostatic interaction with the negative charges placed on the phosphate groups of the DNA skeleton reducing their intercalation capability (see below).

(iv) Harmine derivatives (**3a–3d**) showed the highest photosensitizing efficiency. *I. e.*, the photosensitizer's concentration (absorbance) needed to induce the same amount of DNA-damage was one or two orders of magnitude lower than the required concentration for the corresponding *N*-methyl-nor-harmane (**1a–1d**) and *N*-methyl-harmane (**2a–2d**). Therefore, the methoxy group at C(7) enhances the overall photosensitizing activity of the  $\beta$ C-ring. This could be a consequence of an increased capability to generate ROS<sup>7</sup> and/or of an increased binding affinity to DNA (Fig. 1).

### Interaction between *N*-methyl- $\beta$ Cs and calf thymus DNA

**Re-examination of the molar absorption coefficient for ctDNA.** ctDNA is a good model for mammalian double-stranded DNA. For that reason, it has been widely used in several quantitative studies such as the analysis of DNA binding of anticancer drugs<sup>37,38,40,61</sup> and/or the influence of agents on hybridization. UV-visible absorption spectroscopy provides bases for determining concentrations of different analytes, including nucleic acids. In consequence, appropriate and well defined molar absorption coefficient ( $\epsilon$ ) values for the analytes are of extreme importance.

Due to the varying content of water and counter ions,  $\epsilon$  of nucleic acids cannot reliably be based on weight. Many years ago, Chargaff *et al.*<sup>62</sup> introduced a highly accurate method based on the fact that nucleic acids contain one phosphorus atom per nitrogenous base. As such, the absorbance of a given solution of nucleic acid can directly be related to the nucleobase concentration by measuring the total phosphorus content. Based on this method, Felsenfeld *et al.*<sup>63</sup> and Hirschman *et al.*<sup>64</sup> reported (more than 60 years ago) an average value of  $6600 \text{ M}^{-1} \text{ cm}^{-1}$  (or  $13\,200 \text{ Mbp}^{-1} \text{ cm}^{-1}$ , when

expressed in terms of base-pairs) for the molar absorption coefficient of ctDNA at  $260 \text{ nm}$  ( $\epsilon^{260 \text{ nm}}$ ). Although the latter value seems to be considerably underestimated and it varies with the experimental conditions (see ESI†), it is frequently adopted by the scientific community in quantitative studies using almost all types of dsDNA material under different experimental conditions.<sup>65</sup>

In this context, the  $\epsilon^{260 \text{ nm}}$  value for ctDNA reconstituted according to the general recommendation of the fabricant were re-examined and accurately determined herein by using a more sensitive technique (*i.e.*, microwave-plasma-emission atomic spectroscopy). Total phosphorus concentration ([P]) and UV-visible absorption spectra were measured from both dialyzed and non-dialyzed ctDNA samples. To further evaluate potential interferences due to pH or ionic strength changes, stock solutions were diluted in different solvents. All the cases showed a linear trend when depicting the corrected absorbance  $A_{\text{cor}}^{260 \text{ nm}}$  vs. [P] (ESI Fig. 2e†). The corresponding  $\epsilon^{260 \text{ nm}}$  obtained from the slopes are listed in ESI Table 1.†

With the exception of ctDNA dialyzed in milliQ water,  $\epsilon^{260 \text{ nm}}$  observed under all the experimental conditions were the same, within the experimental error ( $\langle \epsilon^{260 \text{ nm}} \rangle = 7.9 (\pm 0.5) \times 10^3 \text{ M}^{-1} \text{ cm}^{-1}$  or  $15.8 \times 10^3 \text{ Mbp}^{-1} \text{ cm}^{-1}$ ). This is reflected in the lack of any substantial change in the normalized spectra (ESI Fig. 2f†), suggesting the absence of significant changes of the ctDNA structure when subject to variation of the local environment (ionic strength and/or type of cations). On the contrary, changes in the UV-visible spectrum observed for dialyzed (in milliQ water) ctDNA material due to denaturation correlates with the highest  $\epsilon^{260 \text{ nm}}$  value observed ( $8.9 (\pm 0.2) \times 10^3 \text{ M}^{-1} \text{ cm}^{-1}$ ).

### Fluorescence quenching of $\beta$ C alkaloids by calf-thymus DNA: steady-state and time-resolved spectroscopy

The extent of DNA photosensitized damage shown above might be modulated by the magnitude and mode of interaction between DNA and the photosensitizers in the electronic ground and/or excited states. It has been demonstrated that small changes of the molecular structure of  $\beta$ Cs, as well as of the environment (solvent and pH) strongly impact the physicochemical and photochemical properties of these alkaloids.<sup>53,60,66–69</sup> To further investigate this influence, titration of *N*-methyl- $\beta$ C solutions with calf thymus DNA (ctDNA) were monitored by fluorescence spectroscopy (Fig. 2 and ESI Fig. 3 to 9†).

Steady-state fluorescence experiments, performed under three different pH conditions, show the same qualitative trend for all the investigated compounds. Briefly, the emission bands (centred at  $\sim 450 \text{ nm}$ ) exhibit significant changes in terms of intensity when [ctDNA] is increased. The corresponding Stern–Volmer plots (*i.e.*,  $I_0/I$  vs. [ctDNA]) showed a linear dependence (Fig. 2). The extent of the interaction, quantified by the slope ( $K_{\text{SS}}$ ) of the Stern–Volmer plot depends on the chemical structure of the  $\beta$ C derivative (Table 2). When comparing these data, the following conclusions can be drawn:



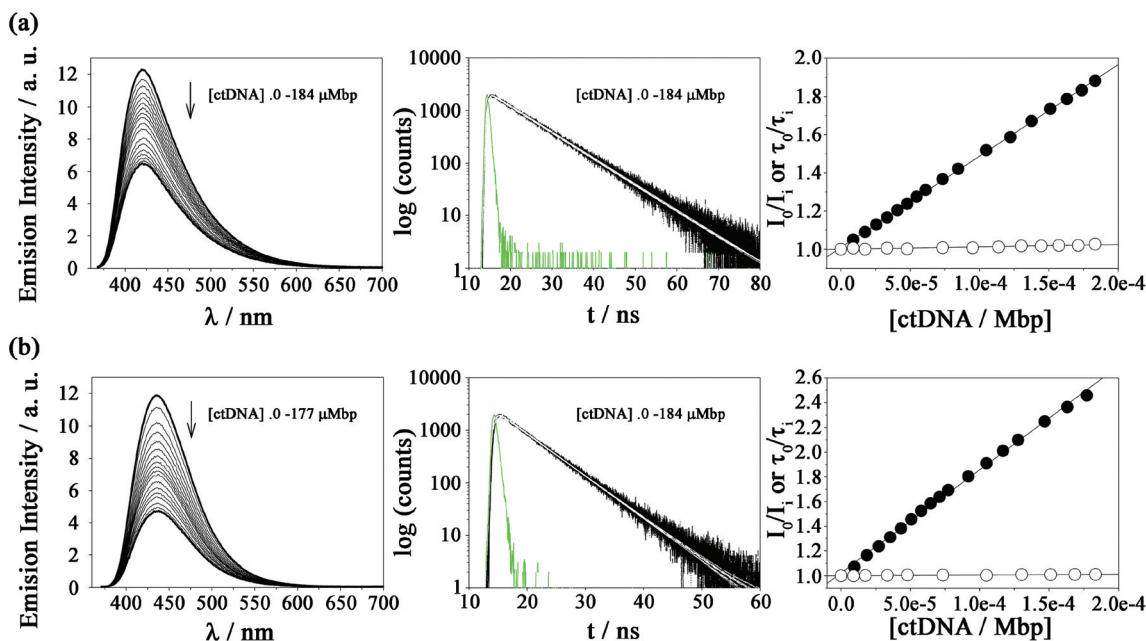


**Fig. 2** Steady-state and time-resolved emission of (a) **3b** (15  $\mu\text{M}$ ) and (b) **3d** (25  $\mu\text{M}$ ) in air-equilibrated buffered solution (pH 7.4), recorded in the presence of increasing amounts of ctDNA ( $\mu\text{Mbp}$ ). Left: corrected emission spectra ( $\lambda_{\text{exc}}$  = 360 nm and 363 nm for **3b** and **3d**, respectively). Arrows indicate the variation in the emission spectra upon increasing [ctDNA] (initial and final concentrations are highlighted in black). Middle:  $\beta\text{C}$  fluorescence decays recorded at wavelengths of the corresponding emission maximum (black lines,  $\lambda_{\text{exc}}$  = 341 nm), prompt signal (green line) and mono-exponential fitting curves (white lines). Right: Stern–Volmer plots of the emission intensities ( $I$ ) (black circles) and lifetimes ( $\tau$ ) (white circles).

**Table 2** Summary of  $\beta\text{Cs}/\text{ctDNA}$  interaction parameters recorded under physiological pH conditions (pH 7.4).  $K_{\text{SS}}$  represents the equilibrium constant for complex formation ( $K_{\text{SS}}$  is the  $K_{\text{SV}}$  value for the static quenching) and  $K_{\text{D}}$  is the dynamic constant

Compound	$K_{\text{SS}} \text{ M}^{-1} \text{ in bp}^{-1} 10^3$	$K_{\text{D}} \text{ M}^{-1} \text{ in bp}^{-1} 10^3$
<b>1a</b>	1.82 ( $\pm 0.03$ )	0.52 ( $\pm 0.02$ ) <sup>a</sup>
<b>1b</b>	0.6 ( $\pm 0.1$ )	0
	0.7 ( $\pm 0.1$ ) (pH 4.8)	
	0.6 ( $\pm 0.1$ ) (pH 9.5)	
<b>1c</b>	2.7 ( $\pm 0.1$ ) <sup>b</sup>	0.25 ( $\pm 0.05$ ) <sup>a</sup>
<b>1d</b>	1.8 ( $\pm 0.1$ )	0
	1.8 ( $\pm 0.1$ ) (pH 4.8)	
	2.5 ( $\pm 0.1$ ) (pH 9.5)	
<b>2a</b>	4.65 ( $\pm 0.03$ )	0.54 ( $\pm 0.02$ ) <sup>a</sup>
<b>2b</b>	2.48 ( $\pm 0.02$ )	0
<b>2c</b>	6.4 ( $\pm 0.7$ ) <sup>b</sup>	0.90 ( $\pm 0.04$ ) <sup>a</sup>
<b>2d</b>	3.7 ( $\pm 0.1$ )	0
<b>3a</b>	7.7 ( $\pm 0.2$ ) <sup>c</sup>	0.33 ( $\pm 0.03$ ) <sup>a</sup>
<b>3b</b>	5.9 ( $\pm 0.3$ )	0
	5 ( $\pm 1$ ) (pH 4.8)	
	6 ( $\pm 1$ ) (pH 9.5)	
<b>3c</b>	16.8 ( $\pm 0.5$ ) <sup>b</sup>	—
<b>3d</b>	9.9 ( $\pm 0.1$ )	0

<sup>a</sup> Data obtained from ref. 38. <sup>b</sup> Data obtained from ref. 40. <sup>c</sup> Data obtained from ref. 39.

(i) The larger the number of substituent (methyl and methoxy groups) in the  $\beta\text{C}$  ring, the larger the overall binding affinity values observed:  $K_{\text{SS}}^{(3\text{a-3d})} > K_{\text{SS}}^{(2\text{a-2d})} > K_{\text{SS}}^{(1\text{a-1d})}$ . DNA can quench a given fluorophore through several deactivation mechanisms. However, in the case of  $\beta\text{Cs}$ , it has been demon-

strated that these alkaloids mainly interact with ctDNA giving rise to the formation of a ground-state static complex ( $\beta\text{Cs}/\text{ctDNA}$ ). In such complexes, the combination of both electrostatic and non-polar forces contributes to the overall interaction. The same mechanism is also expected for quaternary  $\beta\text{C}$  derivatives, **1b**, **2b**, **3b**, **1d**, **2d** and **3d**, (see time-resolved fluorescence data presented below). In consequence, if  $K_{\text{SS}}$  is interpreted as a binding constant, the dependence described above can be ascribed to non-polar contributions: the higher the number of alkyl-substituents, the lower the polarity of the  $\beta\text{C}$ -ring enhancing their hydrophobic interaction (partial intercalation).

(ii)  $N(9)$ -Substituted  $\beta\text{Cs}$  show larger  $K_{\text{SS}}$  values than those observed for  $N(9)$ -unsubstituted derivatives:  $K_{\text{SS}}^{(9\text{-methyl-}\beta\text{Cs})} > K_{\text{SS}}^{(2,9\text{-dimethyl-}\beta\text{Cs})} \gg K_{\text{SS}}^{(\beta\text{Cs})} > K_{\text{SS}}^{(2\text{-methyl-}\beta\text{Cs})}$ . This might well be because of the decrease in the polarity of the  $\beta\text{C}$  ring due to the substitution of the hydrogen atom by the methyl group and, therefore, is more likely to enhance the hydrophobic interaction mode of the  $\beta\text{C}$  ring.

(iii)  $N(2)$ -Substituted  $\beta\text{Cs}$  show  $K_{\text{SS}}$  values slightly lower than those observed for the corresponding  $N(2)$ -unsubstituted derivatives:  $K_{\text{SS}}^{(2,9\text{-dimethyl-}\beta\text{Cs})} < K_{\text{SS}}^{(9\text{-methyl-}\beta\text{Cs})}$  and  $K_{\text{SS}}^{(2\text{-methyl-}\beta\text{Cs})} < K_{\text{SS}}^{(\beta\text{Cs})}$ . This seems counterintuitive since the net positive charge present in quaternary  $\beta\text{Cs}$  should enhance the coulombic attractions with the negatively charged DNA backbone. However, the methyl groups placed at  $N(2)$  might either introduce steric hindrance or block the chance to establish hydrogen bonding between  $\beta\text{Cs}$  and nucleobases. This can explain



the decrease in the overall strength of the interaction observed.

(iv) The dependence of  $K_{SS}$  with the pH has already been demonstrated for  $N(2)$ -unsubstituted- $\beta$ Cs (*i.e.*,  $\beta$ Cs and 9-methyl- $\beta$ Cs): the lower the pH, the higher the binding affinity. The latter fact was accounted for by the fact that under acidic conditions, protonated species of  $N(2)$ -unsubstituted- $\beta$ Cs are present in the solution. Thus, the contribution of electrostatic forces (attraction between the cationic alkaloids and the negatively charged phosphate groups of the DNA) to the overall interaction would be enhanced. On the contrary, the pH-dependence was not observed for quaternary  $\beta$ Cs (**1b**, **2b**, **3b**, **1d**, **2d** and **3d**). This is accounted for by the fact that, in the whole pH-range investigated (4.8–9.5), only one acid–base species of quaternary  $\beta$ Cs is present in the bulk solution.

(v) The presence of ctDNA does not induce changes in the shape or the position of the emission maxima. Thus, the polarity of the environment/surroundings of the fluorophores (at least, with respect to the pyridine ring of the  $\beta$ Cs) is not significantly modified. This confirms, once more, that  $\beta$ Cs are not fully intercalated into the DNA helix.

The almost null contribution of the dynamic quenching to the overall interaction between  $N(2)$ -unsubstituted- $\beta$ Cs and ctDNA has already been demonstrated for related  $\beta$ Cs. To further evaluate potential dynamic contributions to the overall emission quenching described above, fluorescence lifetimes of quaternary  $\beta$ Cs (2-Me- $\beta$ Cs and 2,9-diMe- $\beta$ Cs) were measured in the presence of increasing ctDNA concentrations. Decays shown in Fig. 2, ESI Fig. 7 and 8† were the same in the whole ctDNA concentration range investigated, indicating the lack of dynamic contribution to the overall fluorescence quenching induced by ctDNA. This is also represented in the corresponding Stern–Volmer plot ( $\tau_0/\tau$  vs. [ctDNA]) showing slopes equal to zero (see the dynamic quenching constants,  $K_D$ , listed in Table 2). The data confirm that static interactions dominate the overall interactions between the investigated  $\beta$ Cs and ctDNA.

### Cellular uptake and release of norharmane derivatives

Changes in the  $\beta$ C's chemical structure, including  $N$ -methylation, can modulate both the dynamics of the uptake into cells and/or the specific intracellular localization of the  $\beta$ C. Although cellular uptake of  $\beta$ Cs has been suggested, the fact that these alkaloids exhibit similar spectral patterns to endogenous chromophores makes quite a challenge to univocally establish their precise intracellular localization by using conventional fluorescence microscopy. To further address this, *in vitro* cultures of HeLa and HEK293 cell lines were co-incubated with four different  $\beta$ C derivatives and monitored by FLIM. Compounds **1a–1d** derivatives were used herein as representative examples.

When co-incubated with  $\beta$ Cs in PBS (extracellular [ $\beta$ C] = 10–15  $\mu$ M), cells were able to take up all four investigated compounds within 20 min. All  $\beta$ C derivatives show a similar image pattern, staining the same intracellular structures (Fig. 3).

Interestingly, the compounds present a specific intracellular accumulation pattern (Fig. 3, left column) in some internal structures. Although the accumulation is not specific, it is sufficient to isolate these regions using home-coded macros in Fiji. The second and third columns in Fig. 3 show the lifetime images of the complete cells and from the internal structures where the compounds are accumulated, respectively. Fig. 3 also shows arrows traced where we reconstruct histograms of lifetime and intensity. These histograms show the changes in intensity and lifetime along the arrow traced. For a better clarity, we indicate under grey bars, the increase in fluorescence due to a structure where the compounds are accumulated. As can be observed, the increases in intensity are coincident with lower fluorescence lifetimes. Fig. 3 suggests that all  $\beta$ C derivatives show a similar intensity pattern, due, probably, to a staining of the same intracellular structures. Also, this is in agreement with our previous studies which indicated that fluorescence lifetimes of the compounds are dependent on the environment.<sup>7</sup> This fact, together with the long fluorescence lifetimes of all the compounds, open the possibility to use this parameter to monitor changes in the microenvironment inside these structures and to introduce a time-gate in the decay traces registered in FLIM to discard completely the autofluorescence of cells.

Surprisingly, data also showed that the dynamic of both uptake and release processes strongly depends on the chemical structure of the alkaloid. Briefly, neutral  $\beta$ Cs (**1a** and **1c**) showed a faster uptake than quaternary  $\beta$ Cs (**1b** and **1d**). This is evidenced by the fact that the maximum emission is reached before 5–10 min of incubation with **1c** or **1a** (Fig. 4a and ESI Fig. 10a,† respectively), whereas up to 20 min of incubation were needed for both cationic derivatives (Fig. 4b and ESI Fig. 10b†). Upon washing (two times) the cell cultures with PBS free of  $\beta$ C, a prompt and drastic decrease of the fluorescence intensities of cells preincubated with both neutral derivatives (**1a** and **1c**) was observed, reaching the cell autofluorescence background levels. On the contrary, fluorescence intensity of washed cells pre-incubated with **1b** and **1d** remains nearly constant within the time window of analysis (30 min).

The facts described in the paragraph above are consistent with a free diffusion of **1a** and **1c** between intracellular compartments and the extracellular space. Thus, a passive uptake/release would be the operative mechanism for neutral  $\beta$ Cs. On the contrary, the permeability of the cellular membrane for the polar quaternary  $\beta$ C cations is probably slow, and both processes (uptake and release) may even be mediated by an active transport. These aspects need to be further investigated.

Intracellular localization was further characterized by using two different red fluorescent biomarkers, Mitotracker® and LysoTracker®, that selectively stain mitochondria and lysosome, respectively. To this aim, **1d** was chosen as a representative example, due to its intrinsic photophysical properties setting it aside from all the other investigated compounds including high fluorescent emission quantum yield





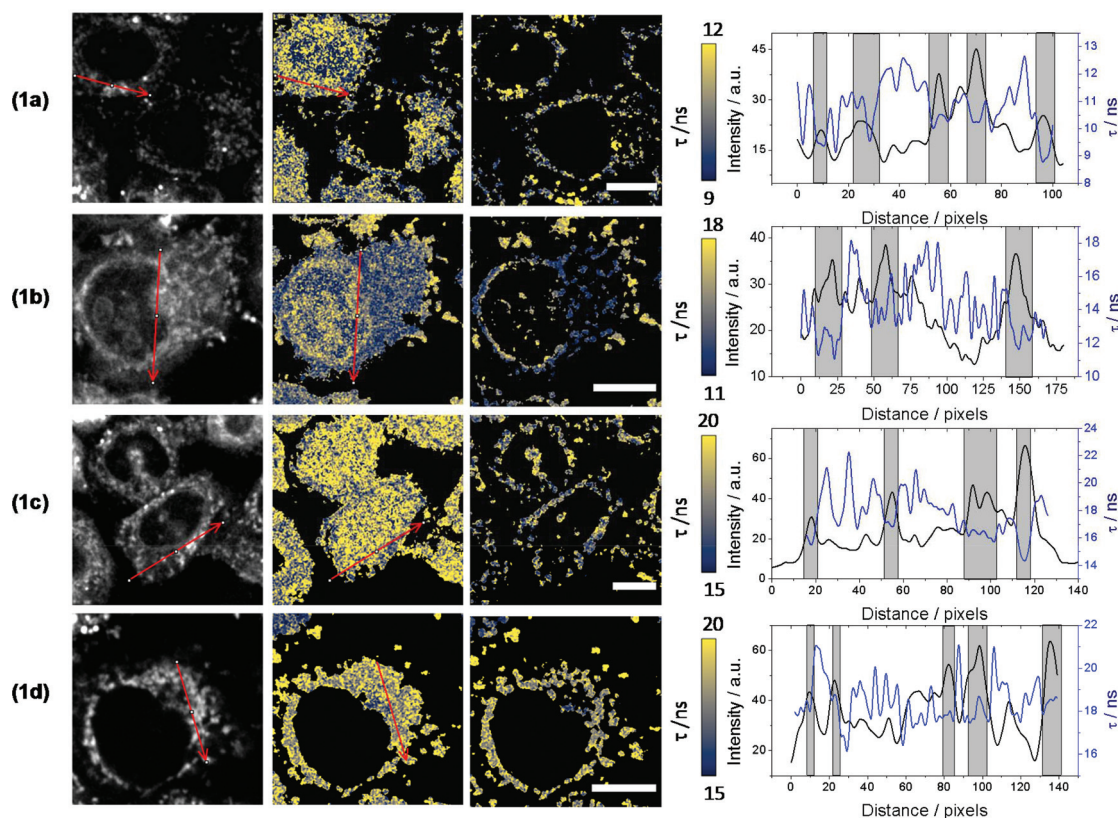


Fig. 3 Fluorescence images of HeLa cells incubated with compounds **1a**, **1b**, **1c** and **1d**. Column 1: fluorescence intensity images of the dye. Column 2: fluorescence lifetime images of dye in the whole cell. Column 3: fluorescence lifetime images in the accumulated intracellular organelles. Scale bar = 10  $\mu\text{m}$ . Column 4: plot of intensities and lifetimes along the selected arrows.

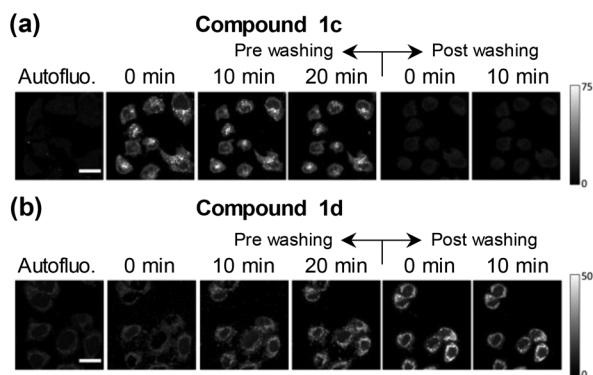


Fig. 4 Examples of fluorescence images obtained from HEK293 cells co-incubated with compounds (a) **1c** and (b) **1d**. Column 1: HEK293 autofluorescence. Columns 2 to 4: fluorescence images obtained after 0, 10 and 20 minutes of addition of the corresponding  $\beta\text{C}$ , respectively. Columns 5 and 6: images obtained 0 and 10 minutes after washing HEK293 cells with PBS. Scale bar = 20  $\mu\text{m}$ .

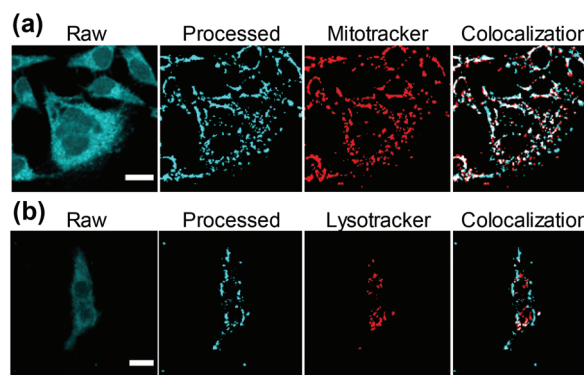


Fig. 5 Fluorescence images of HeLa cells co-incubated with compound **1d** (cyan). The figure shows the raw fluorescence images (first column) and the processed images isolating the regions where the compound accumulates. The two different biomarkers (red): (a) Mitotracker® and (b) LysoTracker® are in the third column. The merge from processed and biomarker images and the colocalization pixels (white) are represented in the fourth column. Scale bar = 20  $\mu\text{m}$ .

( $\Phi_{\text{F}} \sim 0.75$ ), highest fluorescent lifetime ( $\tau_{\text{F}} = 25.9$  ns) and lack of fluorescence pH-dependence.<sup>7</sup> Results show that **1d** is mostly localized in mitochondria (Fig. 5a and ESI Fig. 11†). This is better represented by the white pixels in the colocalized image. Moreover, a Pearson's coefficient value,  $r$ , of  $0.65 \pm 0.03$

was obtained (see ESI†), indicating the dye is mainly localized in mitochondria. In contrast, the relatively low Pearson's coefficient ( $0.25 \pm 0.02$ ) calculated from LysoTracker® images (Fig. 5b and ESI Fig. 12†) suggest a low or null internalization into the lysosomes.



## Conclusions

The study describes the structural and mechanistic basis underlying the photosensitizing properties and the cellular distribution of a selected group of *N*-methyl- $\beta$ C alkaloids (Table 1). Data clearly show that small changes in the chemical structure of the  $\beta$ C ring allow a fine-tuning of its intrinsic physicochemical properties, enabling specific responses and/or applications. Briefly,

(a) methylation enhances its photosensitizing properties either by increasing its binding affinity with macromolecules such as DNA and/or by increasing its oxidation potential. The latter fact is (indirectly) evidenced by the DNA photodamage spectra induced by these derivatives. With the exception of **3b**, all the *N*-methyl derivatives investigated showed a quite selective damage generation, where oxidized purines represent the major type of photoproducts formed.

(b) The quite interesting photochemical and photosensitizing properties of *N*-methyl- $\beta$ Cs (*i. e.*, the bathochromic shift of the absorption bands as well as the enhancement on the photosensitizing properties induced by methylation) make these derivatives suitable for different biotechnological applications. *N*(9)-Methyl- $\beta$ Cs could represent excellent candidates for the development of novel and more efficient albumin-folate- $\beta$ C conjugates as selective vehicles for tumour cell targeted PDT.<sup>45</sup>

(c) Our data demonstrate that all the investigated compounds are taken up by HeLa and HEK293 cells. Data reveal that:

(i) lifetime changes depend on the microenvironment. This can have particular ramifications providing an open future for the development of biotechnological applications based on small molecules derived from  $\beta$ C chemical structures.<sup>70</sup>

(ii) These compounds mainly accumulate into mitochondria. Therefore, although other intracellular components could be involved, mitochondrial DNA could be an important target for the  $\beta$ C-mediated photoinactivation.

(iii) Neutral  $\beta$ Cs show a faster uptake and release kinetic than the quaternary derivatives, suggesting that different cellular uptake pathways (or mechanisms) might operate in each case. This distinctive dynamic pattern observed provides valuable information to further understand some of the biological effects described in the introductory section. In particular, they can help to understand/assess the neurotoxic effect of quaternary  $\beta$ Cs played at the mitochondrial domain. Also, these results shed light into the mechanism of anti-parasitic<sup>22</sup> and antiviral<sup>35</sup> activity of **1c**, **2c** and **3c**.

(d) As a secondary outcome of this study, accurate absorption coefficients of ctDNA under different conditions were established. Values were determined by using a more sensitive technique (*i. e.*, microwave-plasma-emission atomic spectroscopy) than previously applied. The greater accuracy of the new values is expected to have a strong impact on binding constants measurements, quantitative real-time PCR,<sup>71</sup> among others. In this regard, values reported herein might represent an excellent alternative to standardize the preparation and quantification of ctDNA solutions.

## Conflicts of interest

There are no conflicts to declare.

## Acknowledgements

This research was funded by Grants PICT-2015-0374, 2016-0370 and 2018-3193 (ANPCyT, Argentina), and CTQ2017-85658-R and CTQ2014-55474-C2-2-R (Spanish Ministry of Economy and Competitiveness). MPD and FMC are research members of CONICET. Authors thanks to Carlos G. Alberici for his technical support, and Fernando Villarruel for the artwork.

## Notes and references

- J. Torreilles, M. C. Guerin and A. Previero, *Biochimie*, 1985, **67**, 929–947.
- J. Adachi, Y. Mizoi, T. Naito, Y. Ogawa, Y. Uetani and I. Ninomiya, *J. Nutr.*, 1991, **121**, 646–652.
- S. Manabe, J. Yuan, T. Takahashi and R. C. Urban Jr., *Exp. Eye Res.*, 1996, **63**, 179–186.
- K. Pari, C. S. Sundari, S. Chandani and D. Balasubramanian, *J. Biol. Chem.*, 2000, **275**, 2455–2462.
- R. Spijkerman, R. van den Eijnden, D. van de Mheen, I. Bongers and D. Fekkes, *Eur. Neuropsychopharmacol.*, 2002, **12**, 61–71.
- U. Breyer-Pfaff, G. Wiatr, I. Stevens, H. Jörg Gaertner, G. Mundle and K. Mann, *Life Sci.*, 1996, **58**, 1425–1432.
- F. A. O. Rasse-Suriani, F. S. García-Einschlag, M. Rafti, T. Schmidt De León, P. M. David Gara, R. Erra-Balsells and F. M. Cabrerizo, *Photochem. Photobiol.*, 2018, **94**, 36–51.
- C. Liu, M. N. Masuno, J. B. MacMillan and T. F. Molinski, *Angew. Chem., Int. Ed.*, 2004, **43**, 5951–5954.
- J. Stöckigt, A. P. Antonchick, F. Wu and H. Waldmann, *Angew. Chem., Int. Ed.*, 2011, **50**, 8538–8564.
- Q. Chen, C. Ji, Y. Song, H. Huang, J. Ma, X. Tian and J. Ju, *Angew. Chem., Int. Ed.*, 2013, **52**, 9980–9984.
- D. Pressnitz, E.-M. Fischereder, J. Pletz, C. Kofler, L. Hammerer, K. Hiebler, H. Lechner, N. Richter, E. Eger and W. Kroutil, *Angew. Chem., Int. Ed.*, 2018, **57**, 10683–10687.
- B. Greiner, C. Fahndrich, S. Strauss and H. Rommelspacher, *Naunyn-Schmiedeberg's Arch. Pharmacol.*, 1983, **322**, 140–146.
- D. Fekkes and W. T. Bode, *Life Sci.*, 1993, **52**, 2045–2054.
- M. G. Thomas, D. Sartini, M. Emanuelli, M. J. van Haren, N. I. Martin, D. M. Mountford, D. J. Barlow, F. Klamt, D. B. Ramsden, M. Reza and R. B. Parsons, *Biochem. J.*, 2016, **473**, 3253–3267.
- M. A. Collins and E. J. Neafsey, in *Neurotoxic Factors in Parkinson's Disease and Related Disorders*, ed. A. Storch and M. A. Collins, Kluwer Academic/Plenum Publishers, New York, 2000, pp. 115–129.
- D. A. Gearhart, M. A. Collins, J. M. Lee and E. J. Neafsey, *Neurobiol. Dis.*, 2000, **7**, 201–211.



- 17 D. A. Gearhart, E. J. Neafsey and M. A. Collins, *Neurochem. Int.*, 2002, **40**, 611–620.
- 18 R. Albores, E. J. Neafsey, G. Drucker, J. Z. Fields and M. A. Collins, *Proc. Natl. Acad. Sci. U. S. A.*, 1990, **87**, 9368–9372.
- 19 Y. Tadokoro, T. Nishikawa, T. Ichimori, S. Matsunaga, M. J. Fujita and R. Sakai, *ACS Omega*, 2017, **2**, 1074–1080.
- 20 J. Hamann, C. Wernicke, J. Lehmann, H. Reichmann, H. Rommelspacher and G. Gille, *Neurochem. Int.*, 2008, **52**, 688–700.
- 21 R. Cao, Q. Chen, X. Hou, H. Chen, H. Guan, Y. Ma, W. Peng and A. Xu, *Bioorg. Med. Chem.*, 2004, **12**, 4613–4623.
- 22 M. L. Alomar, F. A. Rasse-Suriani, A. Ganuza, V. M. Coceres, F. M. Cabrerizo and S. O. Angel, *BMC Res. Notes*, 2013, **6**, 193.
- 23 C. Di Giorgio, F. Delmas, E. Ollivier, R. Elias, G. Balansard and P. Timon-David, *Exp. Parasitol.*, 2004, **106**, 67–74.
- 24 B. B. Mishra, R. K. Singh, A. Srivastava, V. J. Tripathi and V. K. Tiwari, *Mini-Rev. Med. Chem.*, 2009, **9**, 107–123.
- 25 S. Lala, S. Pramanick, S. Mukhopadhyay, S. Bandyopadhyay and M. K. Basu, *J. Drug Targeting*, 2004, **12**, 165–175.
- 26 A. Gellis, A. Dumètre, G. Lanzada, S. Hutter, E. Ollivier, P. Vanelle and N. Azas, *Biomed. Pharmacother.*, 2012, **66**, 339–347.
- 27 D. J. McKenna, *Pharmacol. Ther.*, 2004, **102**, 111–129.
- 28 L. T. D. Tonin, M. R. Panice, C. V. Nakamura, K. J. P. Rocha, A. O. D. Santos, T. Ueda-Nakamura, W. F. D. Costa and M. H. Sarragiotto, *Biomed. Pharmacother.*, 2010, **64**, 386–389.
- 29 T. Satou, A. Horiuchi, N. Akao, K. Koike, K. Fujita and T. Nikaido, *Exp. Parasitol.*, 2005, **110**, 134–139.
- 30 G. M. Olmedo, L. Cerioni, M. M. González, F. M. Cabrerizo, V. A. Rapisarda and S. I. Volentini, *Food Microbiol.*, 2017, **62**, 9–14.
- 31 G. M. Olmedo, L. Cerioni, M. M. González, F. M. Cabrerizo, S. I. Volentini and V. A. Rapisarda, *Front. Microbiol.*, 2017, **8**, 347.
- 32 G. Van Baelen, S. Hostyn, L. Dhooghe, P. Tapolcsányi, P. Mátyus, G. Lemièrre, R. Dommissie, M. Kaiser, R. Brun, P. Cos, L. Maes, G. Hajós, Z. Riedl, I. Nagy, B. U. W. Maes and L. Pieters, *Bioorg. Med. Chem.*, 2009, **17**, 7209–7217.
- 33 C. W. Wright, J. D. Phillipson, S. O. Awe, G. C. Kirby, D. C. Warhurst, J. Quetin-Leclercq and L. Angenot, *Phytother. Res.*, 1996, **10**, 361–363.
- 34 J. F. Blom, T. Brüttsch, D. Barbaras, Y. Bethuel, H. H. Locher, C. Hubschwerlen and K. Gademann, *Org. Lett.*, 2006, **8**, 737–740.
- 35 M. M. Gonzalez, F. M. Cabrerizo, A. Baiker, R. Erra-Balsells, A. Osterman, H. Nitschko and M. G. Vizoso-Pinto, *Int. J. Antimicrob. Agents*, 2018, **52**, 459–468.
- 36 P. Bag, D. Ojha, H. Mukherjee, U. C. Halder, S. Mondal, A. Biswas, A. Sharon, L. Van Kaer, S. Chakrabarty, G. Das, D. Mitra and D. Chattopadhyay, *Antiviral Res.*, 2014, **105**, 126–134.
- 37 M. M. Gonzalez, M. Pellon-Maison, M. A. Ales-Gandolfo, M. R. Gonzalez-Baró, R. Erra-Balsells and F. M. Cabrerizo, *Org. Biomol. Chem.*, 2010, **8**, 2543–2552.
- 38 M. M. Gonzalez, M. Vignoni, M. Pellon-Maison, M. A. Ales-Gandolfo, M. R. Gonzalez-Baro, R. Erra-Balsells, B. Epe and F. M. Cabrerizo, *Org. Biomol. Chem.*, 2012, **10**, 1807–1819.
- 39 J. G. Yaňuk, M. P. Denofrio, F. A. O. Rasse-Suriani, F. D. Villarruel, F. Fassetta, F. S. García Einschlag, R. Erra-Balsells, B. Epe and F. M. Cabrerizo, *Org. Biomol. Chem.*, 2018, **16**, 2170–2184.
- 40 M. Vignoni, F. A. O. Rasse-Suriani, K. Butzbach, R. Erra-Balsells, B. Epe and F. M. Cabrerizo, *Org. Biomol. Chem.*, 2013, **11**, 5300–5309.
- 41 M. Caprasse and C. Houssier, *Biochimie*, 1983, **65**, 157–167.
- 42 M. M. Gonzalez, F. A. O. Rasse-Suriani, C. A. Franca, R. Pis Diez, Y. Gholipour, H. Nonami, R. Erra-Balsells and F. M. Cabrerizo, *Org. Biomol. Chem.*, 2012, **10**, 9359–9372.
- 43 M. M. Gonzalez, M. P. Denofrio, F. S. Garcia Einschlag, C. A. Franca, R. Pis Diez, R. Erra-Balsells and F. M. Cabrerizo, *Phys. Chem. Chem. Phys.*, 2014, **16**, 16547–16562.
- 44 M. Vignoni, R. Erra-Balsells, B. Epe and F. M. Cabrerizo, *J. Photochem. Photobiol., B*, 2014, **132**, 66–71.
- 45 K. Butzbach, F. A. O. Rasse-Suriani, M. M. Gonzalez, F. M. Cabrerizo and B. Epe, *Photochem. Photobiol.*, 2016, **92**, 611–619.
- 46 J. G. Yaňuk, M. L. Alomar, M. M. Gonzalez, F. Simon, R. Erra-Balsells, M. Rafti and F. M. Cabrerizo, *Phys. Chem. Chem. Phys.*, 2015, **17**, 12462–12465.
- 47 M. Salditt, S. N. Braunstein, R. D. Camerini-Otero and R. M. Franklin, *Virology*, 1972, **48**, 259–262.
- 48 S. Boiteux, T. R. O'Connor, F. Lederer, A. Gouyette and J. Laval, *J. Biol. Chem.*, 1990, **265**, 3916–3922.
- 49 E. Müller, S. Boiteux, R. P. Cunningham and B. Epe, *Nucleic Acids Res.*, 1990, **18**, 5969–5973.
- 50 Milli-Q water was used as dialysis solvent in order to ensure a complete removal of phosphate ions that might initially be provided by the starting ctDNA material.
- 51 Dialysis at fix pH and ionic strength was performed using ammonium chloride buffer (10 mM, pH 7.4) due to its null interference with the analytical methods. Note that the detector of the MP-EAS equipment is not sensitive to chloride ions and, on the other hand, ammonium ions are evaporated in the torch prior to reaching the detector.
- 52 M. J. Cavaluzzi and P. N. Borer, *Nucleic Acids Res.*, 2004, **32**, e13–e13.
- 53 M. M. Gonzalez, J. Arnbjerg, M. Paula Denofrio, R. Erra-Balsells, P. R. Ogilby and F. M. Cabrerizo, *J. Phys. Chem. A*, 2009, **113**, 6648–6656.
- 54 B. Epe, J. Hegler and P. Lester, in *Methods Enzymol.*, Academic Press, 1994, vol. 234, pp. 122–131.
- 55 B. Epe, *Photochem. Photobiol. Sci.*, 2012, **11**, 98–106.
- 56 J. Schindelin, I. Arganda-Carreras, E. Frise, V. Kaynig, M. Longair, T. Pietzsch, S. Preibisch, C. Rueden, S. Saalfeld, B. Schmid, J.-Y. Tinevez, D. J. White, V. Hartenstein, K. Eliceiri, P. Tomancak and A. Cardona, *Nat. Methods*, 2012, **9**, 676–682.
- 57 I. Maisuls, F. M. Cabrerizo, P. M. David-Gara, B. Epe and G. T. Ruiz, *Chem. – Eur. J.*, 2018, **24**, 12902–12911.



- 58 J. G. Yañuk, F. M. Cabrerizo, F. G. Dellatorre and M. F. Cerdá, *Energy Rep.*, 2020, **6**, 25–36.
- 59 V. Lhiaubet-Vallet, M. C. Cuquerella, J. V. Castell, F. Bosca and M. A. Miranda, *J. Phys. Chem. B*, 2007, **111**, 7409–7414.
- 60 F. A. O. Rasse-Suriani, M. Paula Denofrio, J. G. Yañuk, M. Micaela Gonzalez, E. Wolcan, M. Seifermann, R. Erra-Balsells and F. M. Cabrerizo, *Phys. Chem. Chem. Phys.*, 2016, **18**, 886–900.
- 61 A. Prisecaru, Z. Molphy, R. G. Kipping, E. J. Peterson, Y. Qu, A. Kellett and N. P. Farrell, *Nucleic Acids Res.*, 2014, **42**, 13474–13487.
- 62 S. Zamenhof and E. Chargaff, *J. Biol. Chem.*, 1949, **178**, 531–532.
- 63 G. Felsenfeld and S. Z. Hirschman, *J. Mol. Biol.*, 1965, **13**, 407–427.
- 64 S. Z. Hirschman and G. Felsenfeld, *J. Mol. Biol.*, 1966, **16**, 347–358.
- 65 Note that Felsenfeld's (1965) and Hirschman's (1966) manuscripts have been cited ~120 and ~80 times, respectively. In addition, according to one of the world's most popular internet search engines, more than 2,390,000 and 215,000 results match with the searches of "DNA + 6600" and "DNA + 13200", respectively.
- 66 M. M. Gonzalez, M. L. Salum, Y. Gholipour, F. M. Cabrerizo and R. Erra-Balsells, *Photochem. Photobiol. Sci.*, 2009, **8**, 1139–1149.
- 67 F. M. Cabrerizo, J. Arnbjerg, M. P. Denofrio, R. Erra-Balsells and P. R. Ogilby, *ChemPhysChem*, 2010, **11**, 796–798.
- 68 D. Hrsak, L. Holmegaard, A. S. Poulsen, N. H. List, J. Kongsted, M. P. Denofrio, R. Erra-Balsells, F. M. Cabrerizo, O. Christiansen and P. R. Ogilby, *Phys. Chem. Chem. Phys.*, 2015, **17**, 12090–12099.
- 69 O. I. Tarzi, M. A. Ponce, F. M. Cabrerizo, S. M. Bonesi and R. Erra-Balsells, *ARKIVOC*, 2005, **vii**, 295–310.
- 70 S. Hotha, J. C. Yarrow, J. G. Yang, S. Garrett, K. V. Renduchintala, T. U. Mayer and T. M. Kapoor, *Angew. Chem., Int. Ed.*, 2003, **42**, 2379–2382.
- 71 J. L. Love, P. Scholes, B. Gilpin, M. Savill, S. Lin and L. Samuel, *J. Microbiol. Methods*, 2006, **67**, 349–356.

